



HAL
open science

Stoichiometry Controls the Dynamics of Liquid Condensates of Associative Proteins

Pierre Ronceray, Yaojun Zhang, Xichong Liu, Ned Wingreen

► **To cite this version:**

Pierre Ronceray, Yaojun Zhang, Xichong Liu, Ned Wingreen. Stoichiometry Controls the Dynamics of Liquid Condensates of Associative Proteins. *Physical Review Letters*, 2022, 128 (3), pp.038102. 10.1103/PhysRevLett.128.038102 . hal-03838324

HAL Id: hal-03838324

<https://hal.science/hal-03838324>

Submitted on 21 Sep 2023

HAL is a multi-disciplinary open access archive for the deposit and dissemination of scientific research documents, whether they are published or not. The documents may come from teaching and research institutions in France or abroad, or from public or private research centers.

L'archive ouverte pluridisciplinaire **HAL**, est destinée au dépôt et à la diffusion de documents scientifiques de niveau recherche, publiés ou non, émanant des établissements d'enseignement et de recherche français ou étrangers, des laboratoires publics ou privés.



Distributed under a Creative Commons Attribution 4.0 International License

Stoichiometry controls the dynamics of liquid condensates of associative proteins

Pierre Ronceray,^{1,*} Yaojun Zhang,^{1,*} Xichong Liu,^{2,3} and Ned S. Wingreen^{4,5,†}

¹*Center for the Physics of Biological Function, Princeton University*

²*Department of Chemical and Biological Engineering, Princeton University*

³*Stanford University School of Medicine*

⁴*Department of Molecular Biology, Princeton University*

⁵*Lewis-Sigler Institute for Integrative Genomics, Princeton University*

Multivalent associative proteins with strong complementary interactions play a crucial role in phase separation of intracellular liquid condensates. We study the internal dynamics of such “bond-network” condensates comprised of two complementary proteins via scaling analysis and molecular dynamics. We find that when stoichiometry is balanced, relaxation slows down dramatically due to a scarcity of alternative partners following a bond break. This microscopic slow-down strongly affects the bulk diffusivity, viscosity and mixing, which provides a means to experimentally test our predictions.

Protein-rich liquid condensates, also known as membraneless organelles, have recently emerged as an important paradigm for intracellular organization [1–3]. Several distinct molecular mechanisms involved in condensate phase separation have been characterized [4], including weak interactions between intrinsically disordered regions of proteins, interactions with RNA and DNA, and specific protein-to-protein complementary interactions. Here we focus on the latter mechanism, often described in terms of “sticker-and-spacer” models [5], where strongly interacting complementary “stickers” are separated by flexible “spacers”, which have little to no interactions. In a simple case, only two species are involved with complementary sticker domains (Fig. 1a), and the phase-separated liquid consists of a dynamically rearranging network of these bound domains (Fig. 1b). This paradigm of a binary mixture of complementary proteins has been observed in membraneless organelles such as the algal pyrenoid [6], as well as in artificial protein condensates such as SUMO-SIM assemblies [7].

Recent studies show that such binary liquids characterized by strong complementary interactions differ in their properties from usual, non-biological liquids: for instance, their valence sensitively controls their phase boundary through a “magic number” effect [6, 8, 9], and they can exhibit long-lived metastable clusters prior to macroscopic phase separation following a quench [10]. Little is known however about the bulk dynamical properties of these liquids. It is expected that these liquids will inherit some properties of associative polymers—a class of materials characterized by long chains with sparse sticky sites [11]. In these materials, relaxation is slowed down by the attachment-detachment dynamics of binding sites, resulting in *sticky reptation* [12]. However, the corresponding role of attachment-detachment dynamics has not yet been considered in liquid protein condensates.

In this Letter, we study the bulk relaxation mechanisms of liquids consisting of a binary mixture of multivalent complementary proteins (Fig. 1a-b). With theory and simulations, we show that even in such simple

systems, the strong specificity of interactions results in a finely tuned response to changes in composition—a property that cells might exploit to dynamically adapt the mixing properties of condensates. We first present a simple kinetic model that predicts a strong dependence of the local relaxation time of bonds on the composition of the liquid: at equal stoichiometry of complementary domains, we anticipate a sharp peak in the relaxation time. We then employ molecular dynamics simulations to confirm these predictions and show their striking consequences for the bulk diffusivity and the overall viscosity of the liquid. Finally, we demonstrate that this effect quantitatively and qualitatively affects the mixing dynamics of droplets of different compositions, and propose experimental ways to test our theoretical predictions.

Kinetic model for the bond relaxation.

We consider the dense phase of multivalent proteins of two different types, denoted A and B (Fig. 1a), where each domain can bind to one and only one domain of the complementary type. The free energy favoring formation of such a bond is ΔF , with a corresponding unbinding Arrhenius factor $\epsilon = \exp(-\Delta F)$ (we set the thermal energy $k_B T = 1$ throughout). We consider the strong-binding regime, *i.e.* $\epsilon \ll 1$. In this regime, the system at any time looks like a gel-forming network with most bonds between domains satisfied (Fig. 1b). However, over sufficiently long times, bonds still break and rearrange, the system relaxes, and the system can flow as a liquid. We investigate here the dependence of this relaxation time on the Arrhenius factor ϵ and on the composition of the liquid.

In the strong-binding regime, local relaxation is controlled by individual bond breaking (Fig. 1c). This process is slow and thermally activated, occurring at a dissociation rate $k_d = \epsilon/\tau_0$ where τ_0 is a microscopic relaxation time, and these events are rapidly followed by rebinding. However, the two newly unbound complemen-

tary domains are part of the network, and thus are not free: they remain confined and diffuse only in a small volume v_{cage} around their initial position (Fig. 1d). This caging volume is determined by the length and flexibility of linkers. Subsequent to a bond breaking, there is therefore a high probability the two former partners will rebind to each other, thus negating the effect of the bond break on system relaxation. Only if either of the two finds a new, unbound complementary domain within the cage volume (Fig. 1e) does the initial break contribute to system relaxation and liquidity.

If we denote by p the probability that either domain finds a new partner, the effective relaxation time can thus be approximated as $\tau_{\text{rel}} = 1/(pk_d)$. To estimate the probability p , we note that if there are on average n free domains in the volume v_{cage} , the probability of finding a new partner prior to rebinding to the former can be approximated as $p = n/(1+n)$. We can then express $n = v_{\text{cage}}c_{\text{free}}$ in terms of the concentration $c_{\text{free}} = c_A + c_B$ of unbound domains in the system, where we denote by c_A and c_B the respective concentration of free domains of each type. We define the stoichiometry difference $\delta = c_A - c_B$ as the difference between these concentrations (which depends only on the overall composition, not on the fraction bound), and c_{AB} as the concentration of bound domain pairs. We assume that the linkers are sufficiently flexible to consider the binding state of each domain of a protein as independent of the others, and thus treat the binding-unbinding process as a well-mixed solution. The dissociation equilibrium reads $K_d = c_A c_B / c_{AB}$, with K_d the dissociation constant. We thus have:

$$c_{\text{free}} = \sqrt{\delta^2 + 4K_d c_{AB}}. \quad (1)$$

The concentration of free monomers thus exhibits a global minimum at $\delta = 0$ (Fig. 1f).

We relate the dissociation constant to the Arrhenius factor for unbinding, writing $K_d = \epsilon/v_0$ where v_0 is a molecular volume. Indeed, $K_d = k_d/k_a$ where the dissociation rate $k_d = \epsilon/\tau_0$ is proportional to the Arrhenius factor, assuming that the association rate k_a is independent of the binding strength. We can thus express the relaxation time as:

$$\tau_{\text{rel}} = \frac{\tau_0}{\epsilon} \left(1 + \frac{1}{v_{\text{cage}} \sqrt{\delta^2 + 4\epsilon c_{AB}/v_0}} \right). \quad (2)$$

When $n \ll 1$, *i.e.* when there are few available partners within reach of a domain, the second term in Eq. 2 dominates the relaxation time. In particular, τ_{rel} exhibits a sharp maximum at $\delta = 0$, whose magnitude scales as $\tau_{\text{rel}} \propto \epsilon^{-3/2}$. This corresponds to correlated dissociation events: neither of the two domain types is in excess with respect to the other, and so rebinding to a new partner is conditioned on finding another thermally activated unbound domain within v_{cage} . The concentrations of such

unbound domains are $c_A = c_B = \sqrt{K_d c_{AB}} \propto \epsilon^{1/2}$. In contrast, for $\delta \gg 1/v_{\text{cage}}$ such that $n \gg 1$, binding to a new partner is fast and essentially independent of δ , so that $\tau_{\text{rel}} \propto \epsilon^{-1}$. This scaling behavior is our central prediction, and is illustrated in Fig. 1g.

Molecular dynamics simulations.

We employ molecular dynamics simulations to test our theoretical predictions for the relaxation time (Eq. 2). Specifically, we model the system schematized in Fig. 1a-b using a bead-spring representation, where only the binding domains are simulated explicitly (Fig. 2a). Binding between complementary domains is modeled by a soft attractive potential minimized when the beads fully overlap, while strong repulsion between beads of the same

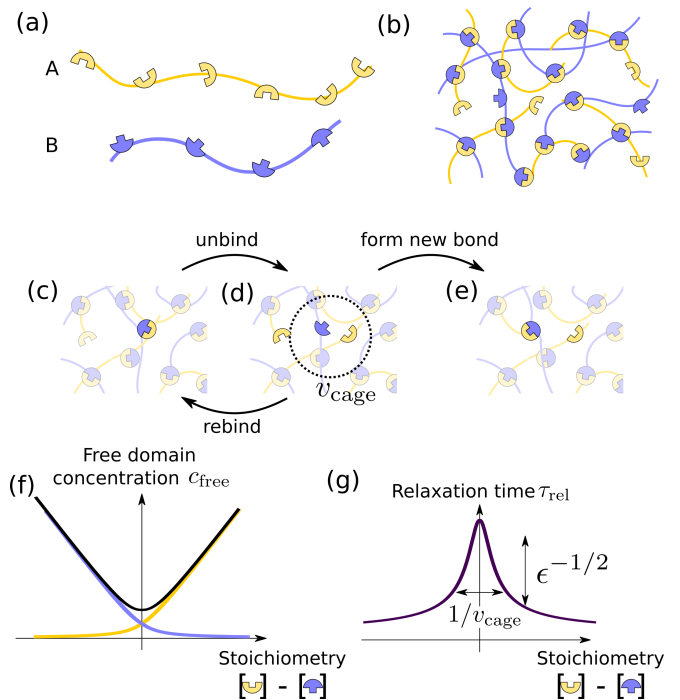


FIG. 1. Stoichiometry controls the bond relaxation time of multivalent associative proteins. (a) Sketch of associative multivalent proteins, with complementary domains separated by flexible linkers. (b) Strong yet reversible binding between proteins leads them to condense into a network with most bonds satisfied. (c-e) Schematic of the bond relaxation mechanism. When two initially bound domains (c) unbind, the two are caged in a small volume v_{cage} (d). Two events can then occur: the initially bound domains can rebind, or, if a free domain is within reach, a new bond may form (e) which is the system's basic relaxation mechanism. (f) Fraction of unbound domains (Eq. 1) of both types as a function of stoichiometry difference. (g) Relaxation time (Eq. 2) corresponding to the process of unbinding and then rebinding with a new partner (c-e), as a function of stoichiometry difference. Here $\epsilon = e^{-\Delta F}$.

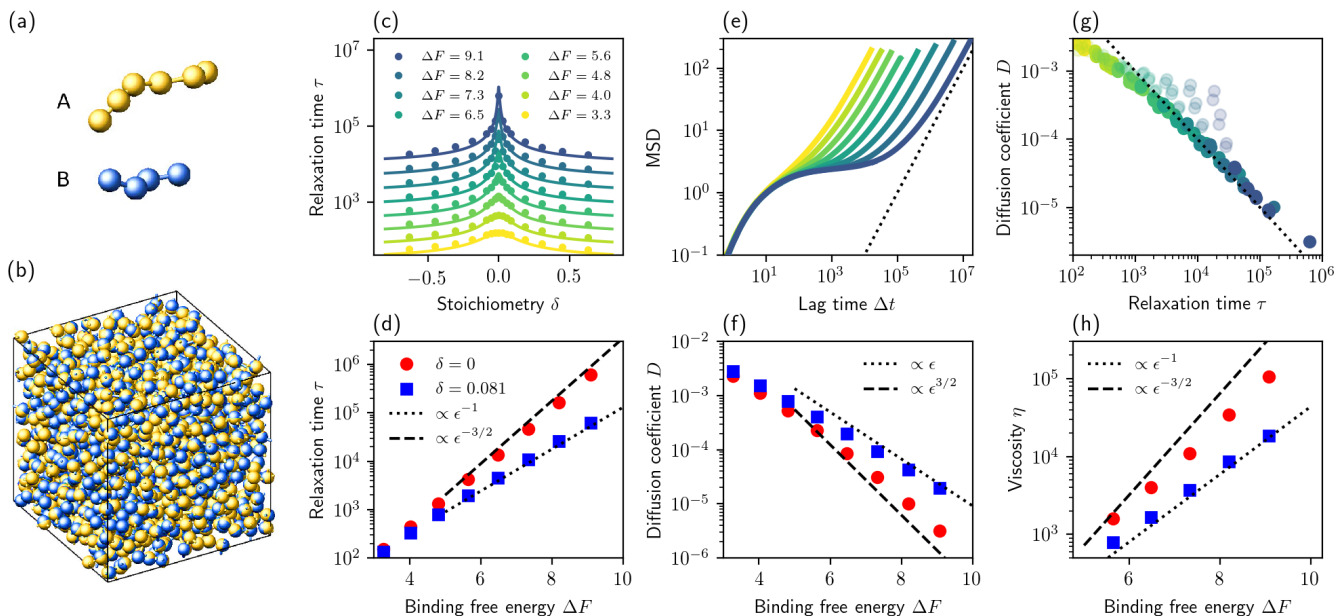


FIG. 2. Molecular Dynamics simulations reveal the importance of stoichiometry to the dynamical properties of the condensate. (a) MD model for the multivalent associative proteins. Colored spheres represent A and B domains. (b) Representative snapshot of the dense, network-forming liquid condensate. (c) Bond relaxation time (see text) as a function of stoichiometry for different binding strengths. Symbols indicate MD simulations; solid curves indicate theory (Eq. 2) with $v_{\text{cage}} = 2.2$ (fitted, consistent with the plateau of MSD in (e)), $\tau_0 = 1.0$ (corresponding to the unbinding time in the absence of any interaction), and $K_d = c_{ACB}/c_{AB}$ measured from data at $\delta = 0$. (d) Bond relaxation time τ_{rel} as a function of binding strength is consistent with predicted scaling for both equal and unequal stoichiometries (Eq. 2, Fig. 1g). (e) Mean squared displacement (MSD) of individual domains as a function of time reveals diffusive scaling (dashed line) at long times (here $\delta = 0$). (f) Diffusion coefficient of the minority species as a function of binding strength at equal and unequal stoichiometry. (g) Diffusion coefficient plotted against bond relaxation time, for all values of δ and ΔF . The dotted black line indicates $D \propto \tau_{\text{rel}}^{-1}$. Transparent circles correspond to systems where one component is in large excess, $|\delta| > 0.2c_{\text{tot}}$, for which disconnected proteins dominates the diffusivity. (h) Viscosity, obtained using the Green-Kubo relation, as a function of binding strength, shows similar scaling to the bond relaxation time (d).

type prevents the formation of multiple bonds involving the same domain (see Methods). The range of the repulsive interaction between domains sets the unit of length, while the unit of time is chosen to be the average time it takes for a free domain to diffuse a unit length. We simulate only the dense phase of this phase-separating system (Fig. 2b). The control parameters are the binding free energy ΔF and the stoichiometric difference $\delta = c_A - c_B$, while the total concentration of domains c_{tot} is held fixed. Simulations are performed using LAMMPS [13, 14] (see Methods).

We first study the relaxation of individual bonds. To quantify this relaxation, we compute the bond adjacency matrix $A_{ij}(t)$, where $A_{ij}(t) = 1$ if domains i and j are bound at time t , and 0 otherwise. We first obtain the average autocorrelation function of this matrix, $C(\Delta t) = \langle \sum_{i,j} A_{ij}(t)A_{ij}(t + \Delta t) \rangle_t$, where the sum runs over all pairs of complementary domains, and then extract the bond relaxation time τ by integration of the normalized autocorrelation, $\tau = \int_0^\infty C(\Delta t)d\Delta t/C(0)$. The resulting relaxation time τ is plotted as a function of stoichiometry difference $\delta = c_A - c_B$ for different values

of ΔF in Fig. 2c (symbols). These values are in good agreement with the theoretical prediction of Eq. 2 (solid curves), and in particular exhibit a clear maximum at equal stoichiometry ($\delta = 0$). The magnitude and sharpness of the peak increases with the binding free energy ΔF . Furthermore, we confirm in Fig. 2d that τ scales as $\epsilon^{-3/2} = \exp(3\Delta F/2)$ at equal stoichiometry, and as $\epsilon^{-1} = \exp(\Delta F)$ at unequal stoichiometry. Thus, the relaxation time increases much faster with ΔF at equal stoichiometry, in agreement with our analytical prediction (Eq. 2).

Diffusivity and viscosity.

How does this sizable difference in relaxation times influence macroscopic condensed-phase properties such as diffusivity and viscosity? To answer these questions, we first monitor the mean squared displacement (MSD) of individual binding domains as a function of lag time (Fig. 2e). Several distinct regimes are apparent in the MSD: short times correspond to bond-level vibrations,

the plateau at intermediate times reveals caging within the bonded network, while the long-time scaling $\text{MSD} \propto \Delta t$ is diffusive, confirming that the system behaves as a liquid. We extract the long-time diffusion coefficient from these simulations, and find that it directly reflects from the bond relaxation time, *i.e.* $D \propto 1/\tau$ (Fig. 2g), and thus scales as $\epsilon^{3/2}$ at equal stoichiometry (Fig. 2f). This shows that the slow bond relaxation within the connected network dominates the diffusive properties of the system. We note however that at large stoichiometry differences ($|\delta| > 0.2c_{\text{tot}}$, transparent symbols in Fig. 2g), fully unbound proteins of the majority species exist and diffuse rapidly through the network, thus violating these scaling laws.

Turning to the viscosity η of the liquid, which we measure using the Green-Kubo relation between viscosity and equilibrium stress fluctuations [15], we observe similarly that $\eta \propto \tau$ (Fig. 2h). The macroscopic transport properties of this binary liquid thus directly reflects the highly stoichiometry-dependent molecular relaxation mechanism illustrated in Fig. 1: in the strong-binding regime, the viscosity of the liquid dramatically increases near equal stoichiometry.

Mixing dynamics.

Our predictions for the dependence of bulk transport coefficients on the stoichiometry of the associative protein condensate have experimentally testable consequences. For instance, by preparing an homogeneous droplet and fluorescently tagging domain on one side, one could measure the mixing dynamics as a function of the composition. We simulate the relaxation of the composition profile for this case by putting in contact two simulation boxes (Fig. 3a-b). We monitor the relaxation of the tagged composition difference between the two halves of the simulation box (Fig. 3c) and extract the relaxation time by exponential fitting of the decay curve (Fig. 3d). Consistent with our equilibrium analysis, we find that mixing is much faster when a species is in excess (Fig. 3d, squares) than when stoichiometry is balanced (Fig. 3d, circles). Interestingly, if the two boxes had initially distinct compositions, mixing is significantly faster: indeed, the gradient of bound fraction of the domain results in a strong chemical potential gradient, and thus in a large thermodynamic force restoring compositional homogeneity.

Discussion.

In this Letter, we investigated the dynamics of protein-rich condensates characterized by strong, specific interactions between complementary binding sites. Our theoretical analysis of the molecular-level relaxation mecha-

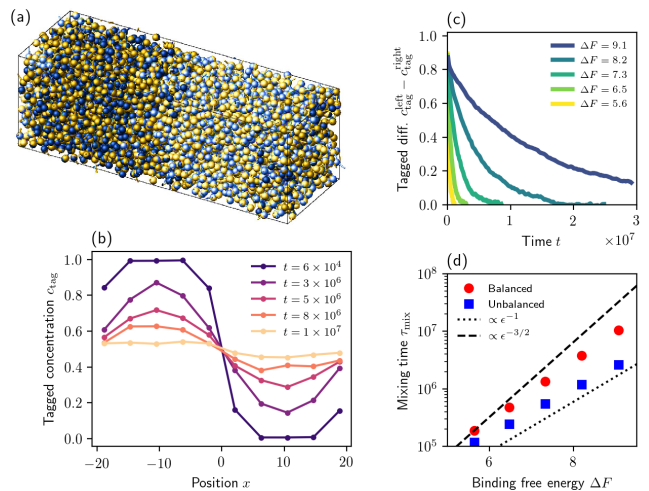


FIG. 3. **Composition controls mixing rate near equal stoichiometry.** (a) Snapshot of an MD simulation with initially tagged particles on the left side of the box. (b) Concentration profiles for tagged particles along the long axis at different times, for equal stoichiometry $\delta = 0$, showing slow relaxation towards the homogeneous state. (c) Relaxation of the tagged concentration difference between the two half-boxes, for variable binding free energy. (d) Equilibration time as a function of binding strength. The unbalanced case has $\delta = 0.061$.

nisms in these liquids suggests a strong composition dependence: near equal stoichiometry of complementary binding sites, the dynamics of the liquid dramatically slows down. This slowing is due to the lack of free binding sites at equal composition, which leads to a predominance of rebinding following bond breaks. We confirmed this mechanism through molecular dynamics simulations and showed that it controls the equilibrium diffusivity and viscosity of the liquid network.

The molecular-level connectivity relaxation of protein liquids through binding-unbinding events is generally not directly accessible in experiments. By contrast, our predictions for macroscopic transport quantities are readily testable, for instance using engineered protein condensates such as SUMO-SIM [7] and SH3-PRM [16] systems. Our predictions would also hold in other liquids characterized by strong specific interactions, such as in highly controllable DNA nanoparticles [17]. In such systems, the effect of composition on diffusivity could be observed using fluorescence recovery after photobleaching [18] as in Fig. 3 and nanoparticle tracking [19], while our predictions on viscosity and mixing dynamics could be tested by monitoring the shape relaxation of merging droplets [20].

While the dynamics of protein condensates can be regulated by many factors, such as density [20, 21], salt concentration, and the presence of RNA [22], our work highlights the possibility that cells can also fine-tune the mechanical and dynamical properties of their membraneless organelles through small changes in composition. Beyond

controlling the time scale of internal mixing and merging of these droplets, stoichiometry-dependent slowing could also impact the mobility exchange rates of “clients” – constituents of the condensates that do not contribute directly to phase separation, but may be functionally important for the cell [3]. Overall, we have shown that high specificity liquids have unusual physical properties and provide novel avenues that cells could use to regulate their phase-separated bodies.

Methods. Molecular Dynamics simulations are performed using the March 2020 version of LAMMPS [13]. Proteins of type A and B are represented by bead-spring multimers with respectively 6 and 4 binding domains (chosen with different valency to avoid magic-number effects associated with the formation of stable dimers [6, 8, 9]). Simulations are done in the NVE ensemble using a Langevin thermostat, with energy normalized so that $k_B T = 1$. Links between domains in a given protein are modeled as finite extensible non-linear elastic bonds, with interaction potential $E(r) = -0.5KR_0^2 \log[1 - (r/R_0)^2]$ as a function of bond elongation r , with coefficients $K = 3$ and $R_0 = 3$. Interaction between domains of the same type are given by a repulsive truncated Lennard-Jones potential, $E(r) = 4\epsilon \left[\left(\frac{\sigma}{r}\right)^{12} - \left(\frac{\sigma}{r}\right)^6 \right]$ with $\epsilon = 1$, $\sigma = 1$ (which sets the unit of length), and cutoff at $R = 2^{1/6}$. Binding between complementary domains occurs via a soft potential, $E(r) = A(1 + \cos(\pi r/r_c))$ for $r < r_c$, with cutoff $r_c = 0.5$. Energy is minimized when domains fully overlap, and Lennard-Jones repulsive interaction between domains of the same type ensured that binding is one-to-one. The interaction strength A is related to the binding free energy by $\Delta F = -\ln\left(\int_0^{r_c} 4\pi r^2 e^{-E(r)} dr / (4\pi r_c^3/3)\right)$. We set the average time it takes for an unbound domain to diffuse a unit length to be the unit of time, $\tau_0 = 1$. The simulation step is $\delta t = 0.0176$. We simulate only the dense phase, with periodic boundary conditions (box size: 14^3 for Fig. 2, $42 \times 14 \times 14$ for Fig. 3) and density typical of a demixed droplet with free surface. The total concentration $c_{\text{tot}} = 1.05$ of domains is kept fixed while the stoichiometry δ is varied.

To ensure equilibration of the system, the attraction strength A is annealed from zero to its final value over a time of 5τ , where τ is the bond relaxation time. The system then evolves for another 5τ , prior to measurements performed over 20τ . In Fig. 2, measurements of τ , MSD, and D have $N = 5$ repeats; measurements of η have $N = 20$. Statistical error bars are smaller than the symbol size. In Fig. 3, the system is initially annealed with walls separating the two halves of the system, with different labels for domains in either side. At $t = 0$, the walls are removed and mixing starts.

Acknowledgments. This work was supported in part by the National Science Foundation, through the Center for the Physics of Biological Function (PHY-

1734030).

* Equal contribution.

† wingreen@princeton.edu

- [1] C. P. Brangwynne, C. R. Eckmann, D. S. Courson, A. Rybarska, C. Hoegel, J. Gharakhani, F. Jülicher, and A. A. Hyman, *Science* **324**, 1729 (2009).
- [2] C. P. Brangwynne, *The Journal of Cell Biology* **203**, 875 (2013).
- [3] S. F. Banani, H. O. Lee, A. A. Hyman, and M. K. Rosen, *Nature Reviews Molecular Cell Biology* **18**, 285 (2017).
- [4] G. L. Dignon, R. B. Best, and J. Mittal, *Annual Review of Physical Chemistry* **71**, 53 (2020).
- [5] J.-M. Choi, A. S. Holehouse, and R. V. Pappu, *Annual Review of Biophysics* **49**, 107 (2020).
- [6] E. S. Freeman Rosenzweig, B. Xu, L. Kuhn Cuellar, A. Martinez-Sanchez, M. Schaffer, M. Strauss, H. N. Cartwright, P. Ronceray, J. M. Plitzko, F. Förster, N. S. Wingreen, B. D. Engel, L. C. M. Mackinder, and M. C. Jonikas, *Cell* **171**, 148 (2017).
- [7] S. F. Banani, A. M. Rice, W. B. Peeples, Y. Lin, S. Jain, R. Parker, and M. K. Rosen, *Cell* **166**, 651 (2016).
- [8] B. Xu, G. He, B. G. Weiner, P. Ronceray, Y. Meir, M. C. Jonikas, and N. S. Wingreen, *Nature Communications* **11**, 1561 (2020).
- [9] Y. Zhang, B. Xu, B. G. Weiner, Y. Meir, and N. S. Wingreen, *bioRxiv*, 2020.08.24.264655 (2020).
- [10] S. Ranganathan and E. I. Shakhnovich, *eLife* **9**, e56159 (2020).
- [11] M. Rubinstein and A. V. Dobrynin, *Trends polym. sci. (Regul. ed.)* **5**, 181 (1997).
- [12] Z. Zhang, Q. Chen, and R. H. Colby, *Soft Matter* **14**, 2961 (2018).
- [13] “LAMMPS Molecular Dynamics Simulator. Available from <https://lammps.sandia.gov/>,”.
- [14] S. Plimpton, *Journal of Computational Physics* **117**, 1 (1995).
- [15] B. D. Todd and P. J. Daivis, *Nonequilibrium Molecular Dynamics: Theory, Algorithms and Applications* (Cambridge University Press, Cambridge, 2017).
- [16] P. Li, S. Banjade, H.-C. Cheng, S. Kim, B. Chen, L. Guo, M. Llaguno, J. V. Hollingsworth, D. S. King, S. F. Banani, P. S. Russo, Q.-X. Jiang, B. T. Nixon, and M. K. Rosen, *Nature* **483**, 336 (2012).
- [17] N. Conrad, T. Kennedy, D. K. Fygenson, and O. A. Saleh, *Proceedings of the National Academy of Sciences* **116**, 7238 (2019).
- [18] N. O. Taylor, M.-T. Wei, H. A. Stone, and C. P. Brangwynne, *Biophysical Journal* **117**, 1285 (2019).
- [19] M. Feric, N. Vaidya, T. S. Harmon, D. M. Mitrea, L. Zhu, T. M. Richardson, R. W. Kriwacki, R. V. Pappu, and C. P. Brangwynne, *Cell* **165**, 1686 (2016).
- [20] A. Ghosh and H.-X. Zhou, *Angewandte Chemie International Edition* **59**, 20837 (2020).
- [21] T. Kaur, I. Alshareedah, W. Wang, J. Ngo, M. M. Moosa, and P. R. Banerjee, *Biomolecules* **9**, 71 (2019).
- [22] S. Elbaum-Garfinkle, Y. Kim, K. Szczepaniak, C. C.-H. Chen, C. R. Eckmann, S. Myong, and C. P. Brangwynne, *Proceedings of the National Academy of Sciences* **112**, 7189 (2015).